Journal of
Materials Chemistry A

Accepted Manuscript

This is an *Accepted Manuscript*, which has been through the RSC Publishing peer review process and has been accepted for publication.

Accepted Manuscripts are published online shortly after acceptance, which is prior to technical editing, formatting and proof reading. This free service from RSC Publishing allows authors to make their results available to the community, in citable form, before publication of the edited article. This *Accepted Manuscript* will be replaced by the edited and formatted *Advance Article* as soon as this is available.

To cite this manuscript please use its permanent Digital Object Identifier (DOI®), which is identical for all formats of publication.

More information about *Accepted Manuscripts* can be found in the **Information for Authors**.

Please note that technical editing may introduce minor changes to the text and/or graphics contained in the manuscript submitted by the author(s) which may alter content, and that the standard **Terms & Conditions** and the **ethical guidelines** that apply to the journal are still applicable. In no event shall the RSC be held responsible for any errors or omissions in these *Accepted Manuscript* manuscripts or any consequences arising from the use of any information contained in them.

In situ sulfur deposition route to obtain sulfur-carbon composite cathodes for lithium-sulfur batteries

W. G. Wang, [a] X. Wang, [a] L. Y. Tian, [a] Y. L. Wang,* [a] and S. H. Ye* [a]

[a]*Institute of New Energy Material Chemistry, Tianjin Key Laboratory of Metal and Molecule Based Material Chemistry, Synergetic Innovation Center of Chemical Science and Engineering (Tianjin), Nankai University, Tianjin 300071, China. Fax:/Tel: +86-22-23500876, E-mail: yeshihai@nankai.edu.cn, ylwang@nankai.edu.cn*

Graphical Abstract

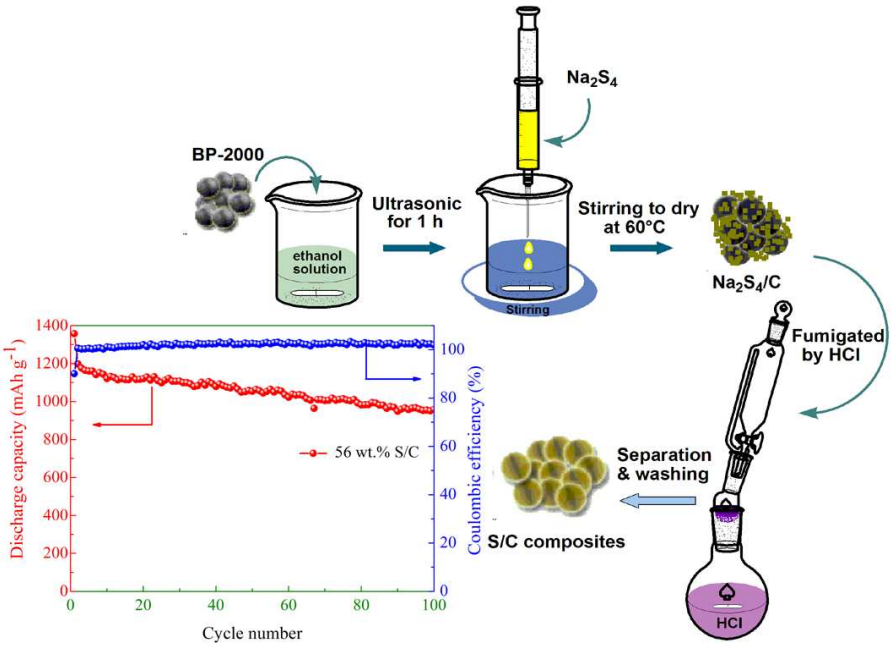

In this work sulfur/carbon composites were prepared by an *in-situ* sulfur deposition route, which has been developed for heterogeneous nucleation of sulfur into the nanopores of conductive carbon black (CCB) by fumigation of Na_2S_4/CCB powder with Hydrochloric acid. The as-prepared sulfur/carbon composites demonstrate enhanced reversible capacity and stable cycle performance.

Journal of Materials Chemistry

Cite this: DOI: 10.1039/c0xx00000x

www.rsc.org/xxxxxx

Paper

In situ sulfur deposition route to obtain sulfur-carbon composite cathodes for lithium-sulfur batteries

W. G. Wang, [a] X. Wang, [a] L. Y. Tian, [a] Y. L. Wang,* [a] and S. H. Ye* [a]

Received (in XXX, XXX) Xth XXXXXXXXX 20XX, Accepted Xth XXXXXXXXX 20XX

DOI: 10.1039/b000000x

An *in situ* sulfur deposition route has been developed for synthesizing sulfur-carbon composites as cathode materials for lithium-sulfur batteries. This facile sythesis method involves the precipitation of most elemental sulfur into the nanopores of conductive carbon black (CCB). The microstructure and morphology of the composites are characterized by means of X-ray diffraction (XRD), scanning electron microscopy (SEM), and transmission electron microscopy (TEM). The results indicate that the most sulfur with amorphous phase are chemically well-dispersed in the nanopores of the CCB. The sulfur content in the composites is confirmed using thermogravimetry analysis (TGA). The S/CCB composites with different sulfur content (52 wt.%, 56 wt.% and 62 wt.%) deliver the remarkably high initial capacities up to 1534.6, 1357.4 and 1185.9 mAh g^{-1} at the current density of 160 mA g^{-1}, respectively. Correspondingly, they maintain stable capacities of 1012.2, 957.9 and 798.6 mAh g^{-1} with the capacity retention over 75.1% after 100 cycles, exhibiting excellent cycle stability. The electrochemical reaction mechanism for the Lithium-sulfur batteries during the discharge process is investigated by electrochemical impedance spectroscopy (EIS). The significantly improved electrochemical performance of the S/CCB composite is attributed to the carbon-wrapped sulfur structure, which suppresses the loss of active material during charging/discharging and the restrained migration of the polysulfide ions to the anode. This facile *in situ* sulfur deposition method represents a low-cost approach to obtain high performance sulfur-carbon composite cathodes for rechargeable lithium-sulfur batteries.

Introduction

Demands for high energy density of rechargeable batteries are ever increasing as the power requirements for newer portable electronic devices, electric vehicles (EVs) and hybrid electric vehicles (HEVs) increase. [1, 2] In this regard, sulfur cathode in lithium sulfur (Li-S) batteries have attracted increasing attention due to its low cost, abundance in nature, environmental friendliness and especially higher theoretical capacity of 1675 mAh g^{-1}, larger theoretical energy density of 2600 Wh Kg^{-1}. [3, 4] Furthermore, An order of magnitude higher capacity than that of the conventional insertion compound cathodes can enable packaged lithium sulfur (Li-S) cells with an energy density of 400-600 Wh kg^{-1}, which is two or three times higher than that of current Li-ion batteries. [5] However, there are still numerous problems that must be overcome for the practical applications of rechargeable lithium sulfur batteries, including the low utilization of active material, the volume change during charge-discharge process, and the poor cycle life, because of the insulating nature of sulfur and the solubility of polysulfides generated during the electrochemical reaction process in the organic based electrolyte. [6-11] Accordingly, to obtain high-performance sulfur cathode, the key issues are how to improve the poor electrically and ionically conductivity of sulfur at room temperature, prohibit the dissolution of polysulfides from the cathode and ensure the well-distribution of sulfur in conductive additives.

Recently, many results have been reported on the improvement of specific capacity and cycle performance of the lithium sulfur batteries. To solve the insulating problem with sulfur, the most frequently adopted current strategy is to modify sulfur cathode, including sulfur-conductive polymer composites, [12-14] and sulfur-porous carbon composites, [15-17] in which sulfur is usually encapsulated to improve the electrical conductivity. Nevertheless, many previously reported conductive carbon matrix involves the using of expensive materials, such as carbon nanotubes, [18, 19] graphene [20-22] and porous carbon fibers, [23, 24] which is likely to offset the advantage of low-cost lithium-sulfur battery. Besides, though the well-designed carbon matrix in the cathode may block the transportation of polysulfides, [24] sulfur is

very difficult to be dispersed into carbon matrix homogeneously. To combat the dissolution of polysulfides in liquid electrolyte, Tarascon et al. [25] present a strategy based on the use of mesoporous chromium trimesate metal organic framework (MOF) as host material for sulfur impregnation to restrain the formation of soluble polysulfide. Cui et al. [5] design a sulfur-TiO_2 yolk-shell nanoarchitecture with internal void space to accommodate the volume expansion of sulfur, resulting in an intact TiO_2 shell to minimize polysulfide dissolution. Furthermore, the electrolyte also can be modified to reduce the solubility of polysulfides. As reported previously, such as addition of $LiNO_3$ [24] and P_2S_5 [26] into organic electrolyte, which can react with metallic lithium to form a rigid passivation layer to reduce the degree of continuous Li_2S precipitation on the Li surface. However, adding these additions above can only prevent further reaction between the lithium polysulphide and the lithium anode, it is unable to inhibit the dissolution of lithium polysulphide into the electrolyte, which results in instability in terms of long cycling. [13, 27] The recent literatures[28, 29] display that a high salt concentration electrolyte is helpful to decrease both the dissolution of lithium polysulphide and the diffusion coefficient of bulky polysulphide in the electrolyte, thus improving the coulombic efficiency.

A sulfur deposition method to synthesize a sulfur-carbon composite for lithium-sulfur batteries has been reported by Wang et al. [15] It exhibited good cyclability and high capacity, while their sulfur deposition process need to be carefully controlled during synthesis, otherwise, the synthesized sulfur nanoparticles can not be highly dispersed in the micro/mesopores of carbon, the discharge capacity of the as-prepared sulfur-carbon composite will decay rapidly. Accordingly, in this work, CCB (Black pearl-2000, Cabot Co.) is used as the substrate for electrode-active materials due to its large specific surface area, pore volume and low cost. An *in situ* sulfur deposition route has been developed for heterogeneous nucleation of sulfur onto CCB via fumigation of Na_2S_4/CCB powder with hydrochloric acid (HCl). Thus sulfur particles are dispersed into carbon matrix homogeneously. Furthermore, high salt concentration electrolyte is used to replace the commercial organic electrolyte. Accordingly, excellent electrochemical performance is obtained for the as-prepared composites.

Experimental

In situ sulfur deposition synthesis of sulfur-carbon composites

The synthesis process for the sulfur-carbon composite via an *in situ* sulfur deposition route is illustrated in Scheme 1, and the reaction formula of *in situ* sulfur deposition method is shown in reaction (1): $Na_2S_4 + 2HCl \rightarrow 2NaCl + H_2S + 3S\downarrow$. CCB, with excellent conductivity and good adsorbability, was used to prepare sulfur-based composites. Firstly, 0.1 g CCB was dispersed in 30 ml ethanol aqueous (10%, v/v) by ultrasonic for 1 h. Afterwards, various amounts of Na_2S_4 aqueous solution (2.0, 3.0 and 4.0 ml, 40 wt.%) were added into the solution above, respectively. Then the mixed solutions were ultrasonically dispersed for 30 m at room temperature followed by stiring to dry at 60 °C in air. After that, the precipitates (Na_2S_4/CCB) were fumigated for 48 h by HCl vapour at 60 °C in an Oil-bathing. Finally, the as-prepared S/CCB composites were washed with anhydrous ethanol and deionized water several times to eliminate salts and impurities and then dried at 60 °C for 12 h in a vacuum oven. And the as-prepared S/CCB composites were heated to 150 °C for 8 h to facilitate diffusion of molten sulfur into the pores of CCB. Then the temperature was increased to 300 °C for 3 h to promote the transform from interpaticle sulfur on the surface of CCB to the absorbed sulfur in the nanopores of CCB. The whole thermal treatment was performed under Ar in a sealed vessel.

Characterization of materials

The sulfur content in the composites was confirmed using TGA (Mettler Toledo, TGA/DSC1) under Ar atmosphere with a flow rate of 50 mL min^{-1} at a heating rate of 10 °C min^{-1} from 30 to 600 °C. The structure of the as-prepared composites was carried out by X-ray diffractometer (Rigaku MiniFlex Ⅱ) and Brunauer-Emmet-Teller (BET, JW-BK 122W). The microstructure and surface morphology of the composites were observed using SEM (Hitachi S-4800), TEM (FEI Tecnai F20) and scanning transmission electron microscopy (STEM). STEM was performed in Tecnai F20 using a high-angle annular dark field (HAADF) detector, coupled with an energy dispersive X-ray spectrometer (EDX).

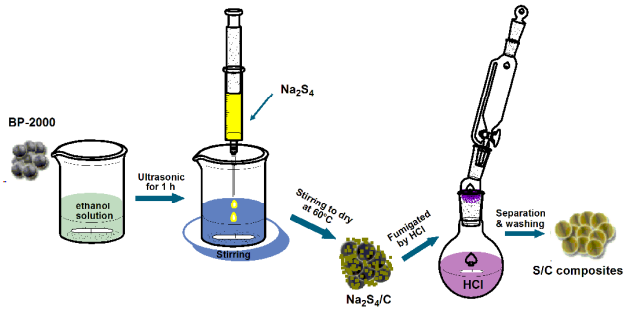

Scheme 1. Scheme illustrating the *in situ* sulfur deposition route to obtain the sulfur-carbon composite.

Electrochemical measurements

The working electrode was prepared by compressing a mixture of the S/CCB composite, acetylene black, and polytetrafluoroethylene (PTFE) in a weight ratio of 70:20:10 with ethanol as a dispersant. The above mixture was spreaded to a thin film on a stainless steel plate, and then punched to a round disk film with 8 mm diameter. The cathode film disk was dried at 60 °C for 12 h. Typical loading of the cathode in the tested batteries was about 1.7~2.5 mg cm^{-2}. The half cells were assembled in a glove box under Ar atmosphere with lithium metal as the counter and reference electrode, and Cellgard 2300 microporous membrane as the separator. $LiN(SO_2CF_3)_2$ (5 M, LiTFSI) and anhydrous lithium nitrate (0.2 M, $LiNO_3$, analytical grade) were dissolved in a mixed solvent of 1,3-dioxolane (DOL) and dimethoxyethane (DME) (1:1, by volume), which was used as the electrolyte. The galvanostatic discharge/charge tests were carried out on a LAND battery system (CT2001C, WuHan Jinnuo, China) at the current density of 160 mA g^{-1} between 1.5 and 3.0 V (vs Li/Li^+) at room temperature. The specific capacities of all test batteries were calculated based on

the weight of sulfur. The cycle voltammetry (CV) was conducted with a LK 2005A electrochemical workstation at a scan rate of 0.1 mV s^{-1} within the voltage range of 1.5 ~ 3.0 V. EIS were measured using a Zahner IM6ex electrochemical workstation in the frequency range of 10 mHz to 100 kHz at potentiostatic signal amplitude of 5 mV. All EIS data are fitted using software Zview with two different equivalent circuits .

Results and discussion

The TG curves and differential thermogravimetric (DTG) curves are shown in Fig. 1. The sulfur content of the S/CCB composites are determined as approximately 52 wt.%, 56 wt.% and 62 wt.%, respectively. The weight loss of the pure sulfur can be observed in a temperature range from 180 to 310 °C, related to the evaporation of sulfur element. All the DTG curves of the three S/CCB composites show two peaks at 180-280 °C and 280-430 °C. The two weight loss processes can be due to different evaporate temperature of two sulfur forms, including interparticle sulfur element at the external surface of the CCB and absorbed sulfur in mesopores or micropores of the S/CCB composites. The higher weight loss temperature of S/CCB composites means the strong adsorption of meso/micropores of the S/CCB composites. [30-32] The most of weight loss is in the temperature range of 280-430 °C, suggesting the most of sulfur is wrapped into the nanopores of carbon substrate.

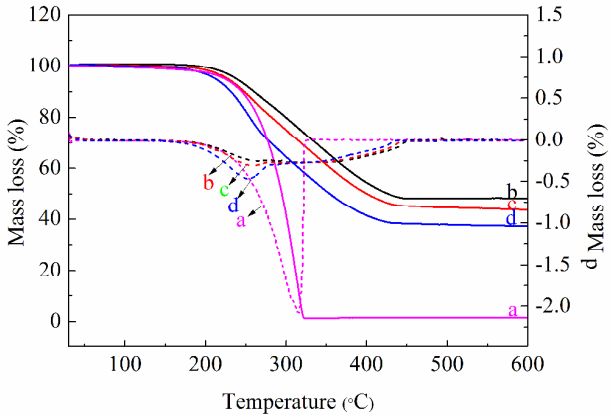

Fig. 1 TG curves and DTG curves of sulfur (a) and the as-prepared S/CCB composites with 52 wt.% S (b), 56 wt.% S (c) and 62 wt.% S (d) recorded under Ar atmosphere with a heating rate of 10 °C min^{-1}.

The Nitrogen adsorption/desorption isothermal curve and the pore distribution of both micropores and mesopores of the CCB are shown in the Fig. S1 (a and b), respectively, indicating that the CCB have well-developed micropores. CCB present a high surface area of 1268.54 m^2 g^{-1} and a large pore volume of 0.94 cm^3 g^{-1} with the predominant pore size around 5.33 nm (Table 1). As calculated below, the maximum sulfur content is 66 wt.% of the S/CCB composite. After loading sulfur into the micropores or mesopores of CCB, the specific surface area of the as-prepared S/CCB composites (Table. 1) decrease rapidly with increasing sulfur content (185.73, 140.35 and 73.19 m^2 g^{-1}, respectively, for the samples with sulfur content of 52%, 56% and 62%). Simultaneously, the corresponding pore volumes decrease to 0.39, 0.28 and 0.16 cm^3 g^{-1}, respectively. It means that the most of nanopores of CCB are occupied by the element sulfur.

Table 1. The specific surface area, pore volume and average pore size of the CCB and the as-prepared S/CCB composites.

Samples	S_{BET} (m^2 g^{-1})	Vt (cm^3 g^{-1})	Average pore size (nm)
CCB	1268.54	0.94	5.33
52 wt.% S/CCB	185.73	0.39	5.23
56 wt.% S/CCB	140.35	0.28	5.07
62 wt.% S/CCB	73.19	0.16	5.53

S_{BET} is the specific surface area and Vt is the total pore volume.

XRD patterns of pure sulfur, CCB substrate and as-prepared S/CCB composites are presented in Fig. 2. One broad diffraction peak located at around 25° can be observed for CCB and all the S/CCB composites. There are no sharp diffraction peaks of crystalline sulfur in all the S/CCB composites, indicating amorphous state of sulfur in the composites. [33, 35] There maybe some interaction between sulfur and CCB. [34] During the heating process, sulfur can melt and diffuse into the nanopores and be trapped inside of the nanopores of CCB at 150 °C due to the lowest viscosity of sulfur and the strong adsorbability of the CCB. Moreover, most interparticle sulfur on the surface of CCB can be sublimed at 300 °C and re-adsorbed into the pores of the CCB. [4, 32] Therefore, the most of element sulfur in the S/CCB composite exists in highly dispersed state, resulting in the amorphous composite. [31, 32] The inset shows XRD patterns of 56 wt.% S/CCB composite at fully charge state after 100 cycles with the charge-discharge current density of 160 mA g^{-1}. The peak located at around 18.1° is attributed to the polytetrafluoroethylene (PTFE) binder in the test electrode plates. A sharp peak around at 22.5° should be related to a crystalline sulfur. It means that crystalline sulfur can regenerate after repeated discharge-charge cycles.

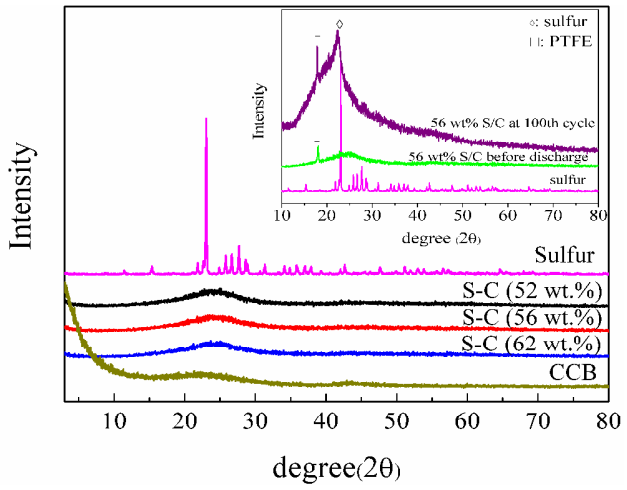

Fig. 2 XRD patterns of pure sulfur, CCB and as-prepared S/CCB composites with different sulfur contents. The inset shows the XRD patterns of 56 wt.% S/CCB composite at fully charge state at the 100th cycle with the charge-discharge current density of 160 mA g^{-1}.

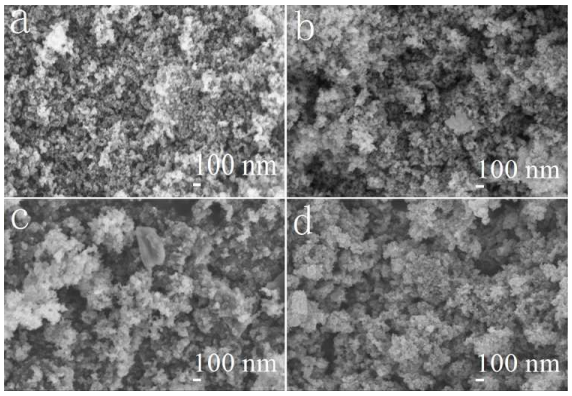

Fig. 3 SEM images of the CCB (a), S/CCB composites with 52 wt.% S (b), 56 wt.% S (c) and 62 wt.% S (d).

Scanning-electron-microscopy (SEM) images of CCB and the as-prepared S/CCB composites are presented in Fig. 3. CCB appears as loose particles aggregation of small carbon spheres with a size of approximately 50 nm in Fig. 3a. After loading sulfur, the sizes of the S/CCB composites particles increase slightly with the increasing of sulfur content. They actually are composed of very fine beaded grains with identical diameter of around 70 ~ 80 nm in Fig. 3 (b-d). There is no obvious difference in morphology for both the as-prepared S/CCB composites and CCB. In addition, no massive or agglomerated sulfur particles are observed. It is possible that the most of active sulfur is diffused and dispersed in the pores of the CCB via the *in-situ* sulfur deposition route and followed heating process. Elemental mapping is used here to evaluate the distribution uniformity of carbon and sulfur in the S/CCB composite in Fig. 4. The elemental composition change of carbon and sulfur elements is detected across a selected area of the S/CCB composites, confirming the existence of sulfur in the S/CCB composites. In particular, it is clear that carbon and sulfur are distributed uniformly in the composite, in agreement with the above XRD and SEM analysis.

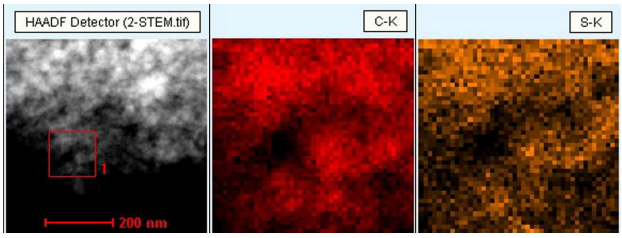

Fig. 4 HAADF-STEM image and corresponding mapping of carbon and sulfur elements across a selected area (red square in STEM) of the as-prepared 56 wt.% S/CCB composite.

To further illustrate the microstructure of as-prepared samples, TEM images are given in Fig. 5. The typical amorphous carbon pattern of CCB can be observed in Fig. 5 (a and b). The nano-particles of CCB interlace to form a chain-like structure. This carbon matrix can ensure good conductivity. For the as-prepared S/CCB composites with different sulfur content, there is no obvious difference in the morphology as shown in Fig.5 (c-e), and no crystalline sulfur can be detected on the surface of amorphous carbon even for the sample with higher sulfur content, indicating that the most of sulfur particles are restrained into the nanopores of CCB with a highly dispersed state. [32] For the composite containing 56 wt.% S at the charged state after 100 cycles at the current density of 160 mA g^{-1}, well-dispersed crystalline sulfur particles with size around 4 nm can be observed, as presented in Fig. 5f. Combined with the results of the XRD patterns, the highly dispersed sulfur nanocrystallines are regenerated from the amorphous sulfur of the as-prepared composites, which should be due to the restriction of micropores of carbon substrate. It is a strong evidence for that most of sulfur are well dispersed into the nanopores of CCB as a result of the uniform size of nanocrystalline of sulfur, especially, as similar as the pore size of the nanopores of CCB.

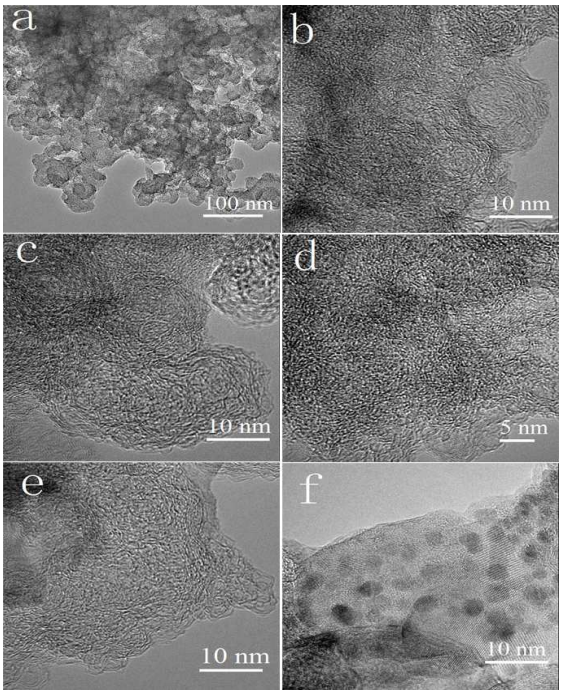

Fig. 5 TEM images of the CCB (a, b) and S/CCB composites with 52 wt.% S (c), 56 wt.% S (d), 62 wt.% S (e) and the composite of 56 wt.% S/CCB at fully charge state at the 100th cycle with the charge-discharge current density of 160 mA g^{-1} (f).

The electrochemical performance of the as-prepared S/CCB composites are investigated in a promising electrolyte system containing $Li[CF_3SO_2)_2N]$ (LiTFSI) and 1,3-dioxolane (DOL), dimethoxyethane (DME) (1:1, by volume) as solvent and 0.2 M lithium nitrate as addition agent. To determine the salt concentration to suitable for this S/CCB composites, the cycle performance of the S/CCB composite with 56 wt.% S in different salt concentration electrolytes (1, 2, 3, 5 and 7 mol·L^{-1}) is investigated, shown in Fig. S2. 5 M is confirmed as the most optimized salt concentration for the S/CCB composites in this lithium-sulfur battery.

Cyclic voltammograms of the S/CCB composites are shown in Fig. 6. The measurement is conducted at a scan rate of 0.1 mV s^{-1} in the voltage range of 1.5-3.0 V (vs Li/Li^+). The peak at different potentials can be attributed to the intrinsic redox reaction of sulfur because CCB only functions as an electron conductor in this operating range. [21] During the first cathodic process, two reduction peaks at 2.15 and 1.85 V (vs Li/Li^+) were observed respectively, which are assigned to the responses of the

two step reactions of sulfur with lithium. The peak around 2.15 V corresponds to the reduction of the element sulfur and the electrolyte to form soluble lithium polysulfide (Li_2S_n, $4 \leq n \leq 8$), [21, 23] as shown in reaction (2): $4Li^+ + 4e^- + S_8 \rightarrow 2Li_2S_4$. [36] The peak around 1.85 V is ascribed to the decomposition of the polysulfide chain in lithium polysulfide to produce insoluble lithium sulfide (Li_2S_2 or Li_2S), [21, 23] as shown in reaction (3): $6Li^+ + 6e^- + Li_2S_4 \rightarrow 4Li_2S$. [36] In addition, a small tailing peak at 1.65 V (vs Li^+/Li) appears during the first discharge process, because the electrochemical reactions between sulfur and lithium need overcome the strong absorbing energy of CCB. This phenomenon can be also observed previously in conductive polymer/sulfur composite materials and sulfur–carbon nano-composites. [33, 37, 38] In the subsequent anodic scan, only one intensive oxidation peak can be observed at approximately 2.46 V, attributed to the complete conversion of Li_2S and polysulfides into elemental sulfur. [39] In the second cycle, the main reduction peaks are shifted to more positive potential and the oxidation peaks are shifted to more negative potential, which is ascribed to polarization of the electrode materials in the first cycle. In the case of samples with sulfur content 52 wt.% and 56 wt.%, there is almost no obvious deference in the peak potential and peak area between the second cycle and subsequent cycles, as shown in Fig. 6 (a and b). It exhibits a relatively good reversibility and capacity retention after the initial electrochemical process. [13] In the case of samples with sulfur content 62 wt.%, there are slight decrease of the peak areas during following cycles in Fig. 6 (c). It implies a slight capacity fading with charge/discharge cycles.

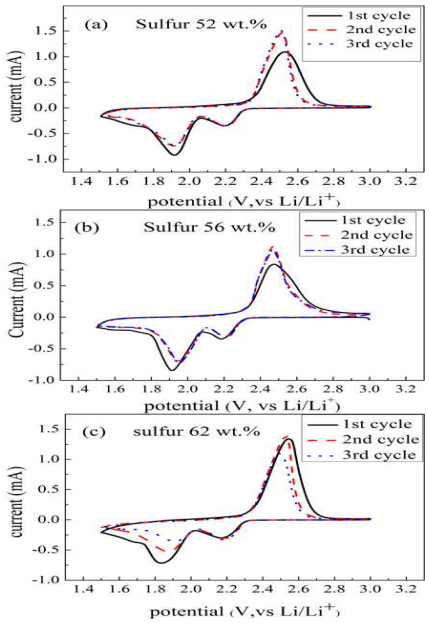

Fig. 6 Cyclic voltammograms of the as-prepared S/CCB composites with 52 wt.% S (a), 56 wt.% S (b), 62 wt.% S (c) at a scan rate of 0.1 mV s^{-1}.

Fig. 7 shows the charge and discharge curves of the as-prepared S/CCB composites at the current density of 160 mA g^{-1}. Two typical discharge voltage plateaus are at ca. 2.25 V and 2.09 V (vs Li/Li^+), in accordance with the CVs in Fig. 6. It is also worth noting that there is a lower potential plateau around 1.73 V in the first discharge processes, consistent with the peaks in the CV curves. It is attributed to the Li-intercalation of absorbed sulfur in the S/CCB composites. During the charge process, only one voltage plateau is observed at 2.31 V (vs. Li/Li^+), attributed to the complete conversion of Li_2S and polysulfides into element sulfur. The overcharge is not observed in the charge curve, indicating that the sulfur shuttle mechanism has been eliminated. It is benefited from the carbon-wrapped sulfur structure of the prepared S/CCB composites via *in-situ* sulfur deposition route, which suppress the loss of active material during charging/discharging. Another reason should be that the migration of the polysulfide ions to the anode is impeded by the high concentration electrolyte.

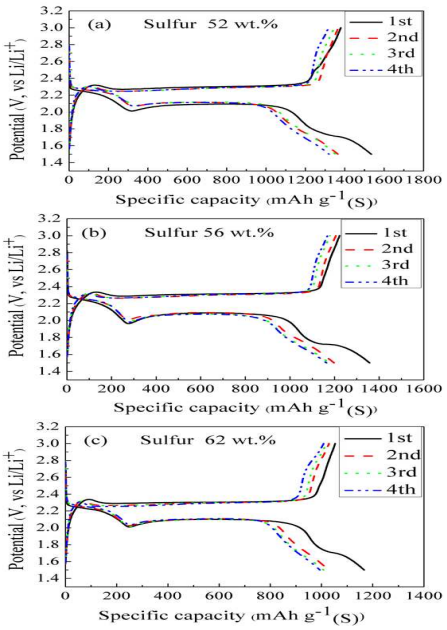

Fig. 7 The initial four charge-discharge curves of the as-prepared S/CCB composites with 52 wt.% S (a), 56 wt.% S (b) and 62 wt.% S (c) at the current density of 160 mA g^{-1}.

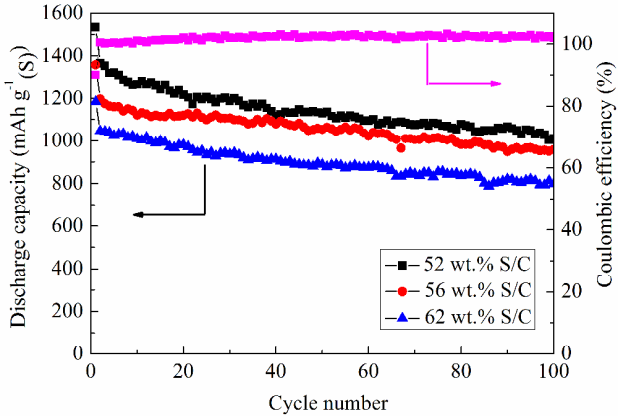

Fig. 8 Cycle performances of the as-prepared S/CCB composites with different sulfur content and the Coulombic efficiency of 56 wt.% S/CCB at the current density of 160 mA g^{-1}

The as-prepared S/CCB composites exhibit high initial discharge capacities and good cycling stability at the current density of 160 mA g^{-1} in Fig. 8. For the sample with 52 wt.% S content, it can achieve high initial capacity of 1534.6 mAh g^{-1}, implying that the active material utilization can be improved while sulfur is well-distributed in the nanopores of CCB. For the

S/CCB composite with 56 wt.% sulfur loading, it has not only a high initial capacity of 1357.4 mAh g^{-1}, but also a high capacity retention of 80.1% after 100 cycles, which is calculated based on the stable discharge capacity in the second cycle. For the material with 62 wt.% S, when the specific capacities were calculated based on the weight of whole S/CCB composites, it also has a higher initial capacity of 711.6 mAh g^{-1} than that of sulfur-carbon composite with 60 wt.% S in the reported literature. [28] Moreover, the coulombic efficiency reaches nearly 100% for the all samples except those in the first cycle, owing to effectively avoiding the polysulphide shuttle effect during the charging process. The S/CCB composites with different sulfur content (52 wt.%, 56 wt.% and 62 wt.%) maintain stable capacities of 1012.2, 957.9 and 798.6 mAh g^{-1} after 100 cycles. Correspondingly, the capacity retention is over 75.1% which is calculated based on the stable cycle capacity of the second cycle (1347.8, 1198.2 and 1047.5 mAh g^{-1}), exhibiting excellent cycle stability.

The rate discharge capability of S/CCB composites is also investigated at discharge current densities of 0.1, 0.2, 0.5 and 1C, which are shown in Fig. 9. The S/CCB composites deliver initial discharge capacity of 1431.9, 1250.3 and 1104.8 mAh g^{-1} of 52 wt.%, 56 wt.% and 62 wt.% S content at 0.1C rate, respectively,. After 40 cycles at varied discharge rates, the reversible discharge capacities can be recovered at 0.1C rate for the all S/CCB composites, indicating good rate cycling stabilities.

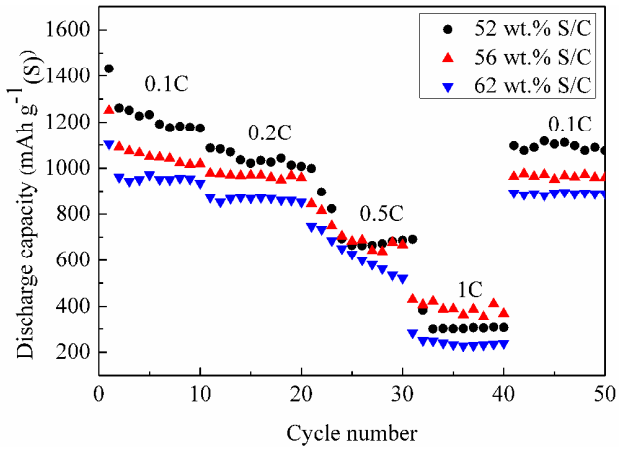

Fig. 9 Rate capabilities of the as-prepared S/CCB composite with 52 wt.%, 56 wt.% and 62 wt.% S content.

Actually, the cycle stability are mainly related to the interfacial charge-transfer process and lithium-ion diffusion in the composite, due to the inescapable aggregation of insulated Li_2S on the cathode surface during cycling. [13] In order to comprehensively understand the reaction mechanism of the as-prepared S/CCB composites synthesized by the *in-situ* sulfur deposition route, EIS of the S/CCB composites at the fully discharged states in different cycles are measured, shown in Fig. 10. In the initial cycles, the impedance spectra are composed of one depressed semicircle in middle frequency regions and a short inclined line (Warburg impedance) in low frequency regions. The semicircle is ascribed to the charge-transfer process at the interface between the electrolyte and sulfur electrode. The Warburg impedance is associated with semi-infinite diffusion. [40] After the initial several cycles, the impedance spectra exhibit two depressed semicircles followed by a long sloping line. The semicircle in the higher frequency region should reflect the interfacial charge transfer process, the semicircle in the lower frequency range could be attributed to the formation of Li_2S (or Li_2S_2) on the carbon matrix in the cathode. [13, 41] Fig. 10 (d and e) present the equivalent circuits used as models to fit the EIS data. *R*s represents the impedance contributed by the resistance of the electrolyte, *R*ct is the charge transfer resistance at the conductive agent interface, CPE is a constant phase element which is used instead of capacitance and R_2 is a deposit diffusion resistance in a thin layer. [13] *Z*w is the Warburg impedance due to the diffusion of the polysulfides within the cathode. [41] *R*ct (Ω mg) and *Z*w (Ω mg) are calculated by multiplying the measured charge-transfer resistance and diffusion impedance with the weight of the active materials (mg) to further illuminate the electrochemical features of the active materials.

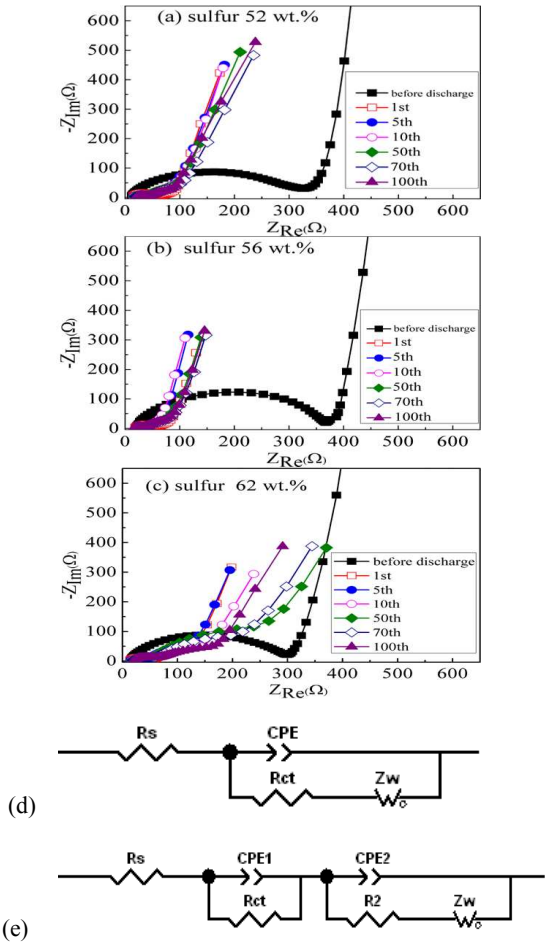

Fig. 10 EIS spectra of the S/CCB composites with 52 wt.% S (a), 56 wt.% S (b) and 62 wt.% S (c) in different cycles after discharging to 1.5 V at a current density of 160 mA g^{-1}. The scatters represent measured data and lines are the fitting curves. Equivalent circuits (d and e) used to fit the experimental data. *R*s is solution resistance, *R*ct is charge-transfer resistance, CPE1 and CPE2 are constant phase element, R_2 and *Z*w are assigned to the resistance in the Li_2S (or Li_2S_2) film and semi-infinite Warburg diffusion impedance of the polysulfides in the cathode, respectively.

The fitting data of EIS using the equivalent circuits are shown in the Table. S1. Before cycling, *R*ct values increase slightly with increasing the sulfur loading (424.9, 433.8 and 446.9 Ω mg

for the samples with 52 wt.%, 56 wt.% and 62 wt.% S content, respectively). During the following five cycles, *R*ct values for the all samples decrease drastically, indicating that an active process may be necessary for the penetration of electrolyte into the electrodes. Simultaneously, the second depressed semicircles occur with cycles, which should be the irreversible deposition and aggregation of insoluble reduction products (Li_2S_2 and Li_2S). In particular, for the sample with 62 wt.% S content, the R_2 value is one order of magnitude bigger than those of other samples, maybe due to a much thicker deposited layer on the surface of sample with 62 wt.% S content. After initial five cycles for the active process, all three samples exhibit stable charge-transfer resistance and stable diffusion impedance, in agreement with their stable cycling performance, shown in Fig. 8. Especially, the sample with 56 wt.% S content owns the lowest charge-transfer resistance and the most stable diffusion impedance during the whole 100 cycles. Correspondingly, it also exhibits the best cycling performance among the three samples.

The huge diffusion impedance mainly resulted from the high concentration electrolyte, is predominant for a major part of the electrochemical reaction process. The migration of the bulky anion such as polysulfide is very slow through the surface passivation layer in the optimized high concentration electrolyte. Thus, the shuttle reaction can be supressed by this way. Benefited from this limitation and well-dispersed of most sulfur element in the nanopores of carbon substrate, the as-prepared S/CCB composites show good electrochemical performance, suggesting that the composites obtained from *in-situ* sulfur deposition route can effectively prevent the sulfur dissolution and enhance active material utilization. This facile in situ sulfur deposition method represents a low-cost approach to obtain high performance sulfur-carbon composite cathodes for rechargeable lithium-sulfur batteries.

Conclusions

An *in situ* sulfur deposition route has been developed for heterogeneous nucleation of sulfur onto CCB by fumigation of Na_2S_4/CCB powder with HCl. This facile synthesis method involves the precipitation of most of elemental sulfur into the nanopores of carbon nanoparticles. The as-prepared S/CCB composites exhibit excellent electrochemical performance. It delivers high initial discharge capacity up to 1534.6, 1357.4 and 1185.9 mAh g^{-1} of S/CCB composites with 52 wt.%, 56 wt.% and 62 wt.% S content, respectively, and preserves at 1012.2, 957.9 and 798.6 mAh g^{-1} after 100 cycles. The capacity retention based on the second cycle capacity (1347.8, 1198.2 and 1047.5 mAh g^{-1}) is 75.1%, 80.1% and 76.2%, respectively. The excellent cycle performance of the as-prepared sulfur-carbon composite can be attributed to that most of sulfur nanoparticles is well dispersed into the meso/micropores of the CCB, which suppresses the loss of active material during charging/discharging and the high concentration of electrolyte impedes the migration of the polysulfide ions to the Li anode. The S/CCB composite synthesized by the simple *in situ* sulfur deposition route is a promising cathode material for rechargeable lithium sulfur batteries.

Acknowledgements

Financial Supports from the 973 Program (2009CB220100), 863 Program (2011AA11A256), and NSFC (51102137) of China are gratefully acknowledged.

Notes and references

[a] *Institute of New Energy Material Chemistry, Tianjin Key Laboratory of Metal and Molecule Based Material Chemistry, Synergetic Innovation Center of Chemical Science and Engineering (Tianjin), Nankai University, Tianjin 300071, China. Fax: +86-22-23500876; Tel: +86-22-23500876; E-mail: yeshihai@nankai.edu.cn, ylwang@nankai.edu.cn*

†Electronic Supplementary Information (ESI) available: The BJH of adsorption isothermal curve and mesopore distributions of CCB. The cyclic performance of as-prepared S/CCB composite with 56 wt.% S in different concentration electrolyte. The fitting data from EIS spectra using the equivalent circuit shown in Fig.10 (d and e) for all the samples. See DOI: 10.1039/b000000x/

1 B. Scrosati and J. Garche, *J. Power Sources*, 2010, **195**, 2419.
2 H. Yamin, J. Penciner, A. Gorenshtain, M. Elam and E. Peled, *J. Power Sources*, 1985, **14**, 129.
3 X. L. Ji, K. T. Lee and L. F. Nazar, *Nat. Mater.*, 2009, **8**, 500.
4 C. Lai, X. P. Gao, B. Zhang, T. Y. Yan and Z. Zhou, *J. Phys. Chem. C*, 2009, **113**, 4712.
5 M. Arumugam, Y. Z. Fu and Y. S. Su, *Acc. Chem. Res.*, 2013, **46**, 1125.
6 R. D. Rauh, K. M. Abraham, G. F. Pearson, J. K. Surprenant and S. B. Brummer, *J. Electrochem. Soc.*, 1979, **126**, 523.
7 E. Peled, Y. Sternberg, A. Gorenshtein and Y. Lavi, *J. Electrochem. Soc.*, 1989, **136**, 1621.
8 H. Yamin, A. Gorenshtein, J. Penciner, Y. Sternberg and E. Peled, *J. Electrochem. Soc.*, 1988, **135**, 1045.
9 H.-S. Ryu, H.-J. Ahn, K.-W. Kim, J.-H. Ahn and J.-Y. Lee, *J. Power Sources*, 2006, **153**, 360.
10 Y. Jung, S. Kim, B.-S. Kim, D.-H. Han, S.-M. Park and J. Kwak, *Int. J. Electrochem. Sci.*, 2008, **3**, 566.
11 S.-E. Cheon, K.-S. Ko, J.-H. Cho, S.-W. Kim, E.-Y. Chin and H.-T. Kim, *J. Electrochem. Soc.*, 2003, **150**, A800.
12 W. Wang, G. C. Li, Q. Wang, G. R. Li, S. H. Ye and X. P. Gao, *J. Electrochem. Soc.*, 2013, **160**, A805.
13 G. C. Li, G. R. Li, S. H. Ye and X. P. Gao, *Adv. Energy Mater.*, 2012, **2**, 1238.
14 L. C. Yin, J. L. Wang, C. Wang, F. J. Lin, J. Yang and Y. N. Nuli, *Energy Environ. Sci.*, 2012, **5**, 6966.
15 C. Wang, J. J. Chen, Y. N. Shi, M. S. Zheng and Q. F. Dong, *Electrochim. Acta*, 2010, **55**, 7010.
16 W. Zheng, Y. W. Liu, X. G. Hu and C. F. Zhang, *Electrochim. Acta*, 2006, **51**, 1330.
17 J. L. Wang, Y. W. Wang, X. M. He, J. G. Ren, C. Y. Jiang and C. R. Wan, *J. Power Sources*, 2004, **138**, 271.
18 J. J. Chen, X. Jia, Q. J. She, C. Wang, Q. Zhang, M. S. Zheng and Q. F. Dong, *Electrochim. Acta*, 2010, **55**, 8062.
19 W. Wei, J. L. Wang, L. J. Zhou, J. Yang, B. Schumann and Y. N. Nuli, *Electrochem. Commun.*, 2011, **13**, 399.
20 J. Z. Wang, L. Lu, M. Choucair, J. A. Stride, X. Xu and H. K. Liu, *J. Power Sources*, 2011, **196**, 7030.
21 Y. Cao, X. Li, I. A. Aksay, J. Lemmon, Z. Nie, Z. Yang and J. Liu, *Phys.Chem. Chem. Phys.*, 2011, **13**, 7660.

22 M. S. Park, J. S. Yu, K. J. Kim, G. Jeong, J. H. Kim, Y. N. Jo, U. Hwang, S. Kang, T. Woo and Y. J. Kim, *Phys. Chem. Chem. Phys.*, 2012. **14**, 6976.

23 G. Y. Zheng, Y. Yang, J. J. Cha, S. S. Hong and Y. Cui, *Nano Lett.*, 2011, **11**, 4462.

24 X. Liang, Z. Y. Wen, Y. Liu, M. F. Wu, J. Jin, H. Zhang and X. W. Wu, *J. Power Sources*, 2011, **196**, 9839.

25 R. Demir-Cakan, M. Morcrette, F. Nouar, C. Davoisne, T. Devic, D. Gonbeau, R. Dominko, C. Serre, G. Ferey and J. M. Tarascon, *J. Am. Chem. Soc.*, 2011, **133**, 16154.

26 Z. Lin, Z. C. Liu, W. J. Fu, N. J. Dudney and C. D. Liang, *Adv. Funct. Mater.*, 2013, **23**, 1064.

27 D. Aurbach, E. Pollak, R. Elazari, G. Salitra, C. S. Kelley and J. Affinito, *J. Electrochem. Soc.*, 2009, **156**, A694.

28 L. Suo, Y. S. Hu, H. Li, M. Armand and L. Chen, *Nat. Commun.*, 2013, **4**, 1481.

29 E. S. Shin, K. Kim, S. H. Oh and W. I. Cho, *Chem. Commun.*, 2013, **49**, 2004.

30 B. Zhang, C. Lai, Z. Zhou and X. P. Gao, *Electrochim. Acta*, 2009, **54**, 3708.

31 B. Zhang, X. Qin, G. R. Li and X. P. Gao, *Energy Environ. Sci.*, 2010, **3**, 1531.

32 G. C. Li, J. J. Hu, G. R. Li, S. H. Ye and X. P. Gao, *J. Power Sources*, 2013, **240**, 598.

33 J. L. Wang, J. Yang, J. Y. Xie, N. X. Xu and Y. Li, *Electrochem. Commun.*, 2002, **4**, 499.

34 J. L. Wang , J. Yang, C. R. Wan, K. Du, J. Y. Xie and N. X. Xu, *Adv. Funct. Mater.*, 2003, **13**, 487.

35 Y. X. Liu, H. Zhan and Y. H. Zhou, *Electrochim. Acta*, 2012, **70**, 241.

36 L. X. Miao, W. K. Wang, A. B. Wang, K. G. Yuan and Y. S. Yang, *J. Mater. Chem. A*, 2013, **1**, 11659.

37 X. M. He, W. H. Pu, J. G. Ren, L. Wang, J. L. Wang, C. Y. Jiang and C. R. Wan, *Electrochim. Acta*, 2007, **52**, 7372.

38 J. L. Wang, L. Liu, Z. J. Ling, J. Yang, C. R. Wan and C. Y. Jiang, *Electrochim. Acta*, 2003, **48**, 1861.

39 L. Ji, M. Rao, H. Zheng, L. Zhang, Y. Li, W. Duan, J. Guo, E. J. Cairns and Y. Zhang, *J. Am. Chem. Soc.*, 2011, **133**, 18522.

40 W. Ahn, K.-B. Kim, K.-N. Jung, K.-H. Shin and C.-S. Jin, *J. Power Sources*, 2012, **202**, 394.

41 L. X. Yuan, X. P. Qiu, L. Q. Chen and W. T. Zhu, *J. Power Sources*, 2009, **189**, 127.

42 Y. S. Su and A. Manthiram, *Electrochim. Acta*, 2012, **77**, 272.